Composites Science and Technology 85 (2013) 17–22

Contents lists available at SciVerse ScienceDirect

Composites Science and Technology

journal homepage: www.elsevier.com/locate/compscitech

Importance of the morphology and structure of the primary aggregates for the dispersibility of carbon nanotubes in polymer melts

M. Salzano de Luna [a], L. Pellegrino [b], M. Daghetta [b], C.V. Mazzocchia [b], D. Acierno [a], G. Filippone [a,*]

[a] Dipartimento di Ingegneria Chimica, dei Materiali e della Produzione Industriale, Università di Napoli Federico II, P.le V. Tecchio, 80, 80125 Naples, Italy
[b] Department of Chemistry, Materials and Chemical Engineering "G. Natta", Politecnico di Milano, Piazza L. da Vinci 32, 20133 Milan, Italy

ARTICLE INFO

Article history:
Received 29 March 2013
Received in revised form 13 May 2013
Accepted 18 May 2013
Available online 1 June 2013

Keywords:
A. Carbon nanotubes
A. Nanocomposites
B. Electrical properties
B. Thermo-mechanical properties
D. Rheology

ABSTRACT

The dispersibility of unfunctionalized multi-walled carbon nanotubes in a polymer matrix is studied focusing on the role of the morphology and structure of the primary aggregates. The particles, synthesized by fluidized bed catalytic chemical vapor deposition and purified through a scalable one-pot method, are dispersed in polystyrene by melt mixing. The filler percolation threshold, assessed through rheological analyses and dielectric spectroscopy, is one order of magnitude lower than that of commercially available nanotubes with similar features. This is ascribed to the hierarchical structure of the primary aggregates, which facilitates both the infiltration of the polymer in the earlier stages of mixing and the pulling out of the nanotubes required for their individualization. The high dispersibility is not achieved to the detriment of the nanotube integrity, and the nanocomposites exhibit enhanced thermal stability and dynamic mechanical properties at low amounts of filler.

1. Introduction

The extremely high stiffness, electrical and thermal conductivity make carbon nanotubes (CNTs) an ideal candidate as filler for polymer nanocomposites (PNCs) of technological interest. The large-scale synthesis of CNTs usually results into bundles of hundreds of microns formed by thousands of individual nanotubes held together by physical entanglements and Van der Waals forces. This prevents an efficient transfer of the CNT superior properties to the nanocomposite. Therefore, the commercial breakthrough of CNT-based nanocomposites requires the overcoming of the difficulties related to the de-agglomeration and dispersion of the primary aggregates during the mixing with the polymer. A good nanoscale dispersion is often related to a low percolation threshold, Φ_c. The latter, however, may hide nanotube breakage that compromises the macroscopic properties of the PNC [1]. On the other hand, higher Φ_c are not necessarily coupled with low performances, the PNC properties being the result of a complex interplay among various features of the nanotubes [2].

Basically, the dispersion of CNTs inside polymer melts starts with the infiltration of polymer chains into the aggregates, which crack and erode, and it ends with the pulling out of single nanotubes in the late stages of the process [3]. To expedite the dispersion, the surface of the nanotubes can be functionalized via a chemical reaction that enhances the affinity with the host polymer and/or reduces the tube-tube attractive forces [4]. On the other hand, dealing with unfunctionalized nanotubes that are themselves easy to disperse would be preferred for a large-scale production of CNT-based nanocomposites [5]. To reach this goal, understanding the influence of the morphological features of the nanotubes and their aggregates in the dispersion process is of crucial importance. Numerous studies have compared the properties of PNCs based on nanotubes prepared through different synthesis methods [6], having different aspect ratios [7,8] and different morphology of the primary aggregates [2,9,10]. A series of focused papers by Pötschke and co-workers ultimately correlated the ease of dispersion of CNTs in polymer melts to a low bulk density of the initial aggregates [11–13]. The relationship, however, is not univocal, the bulk density being only one of many parameters which play a role in determining the actual dispersibility of CNTs [14]. Among others, in this paper we focus on the morphology and structure of the primary aggregate, interpreted as the space arrangement of the nanotubes over various length scales, from the texture of the grain down to the entanglements among the CNTs. More in detail, unfunctionalized multi-walled carbon nanotubes (MWCNTs) have been synthesized by fluidized bed catalytic chemical vapor deposition (FBCCVD) and purified by means of a novel, potentially up-scalable three-step process. The dispersibility in polystyrene (PS) of the resulting powder, whose grains exhibit a

* Corresponding author. Tel.: +39 081 7682104.
E-mail address: gfilippo@unina.it (G. Filippone).

0266-3538
http://dx.doi.org/10.1016/j.compscitech.2013.05.014

peculiar hierarchical structure, has been compared to that of commercially available nanotubes with similar features but differently arranged in the primary aggregates. PS was deliberately selected as its high chain stiffness is known to hinder the infiltration process within the pristine aggregates [3]. PNCs at different particle loading have been prepared through a deliberately mild masterbatch melt mixing route. The state of dispersion of the two kinds of CNTs has been investigated through rheological analyses, dielectric spectroscopy and transmission electron microscopy (TEM). The high dispersibility of the synthesized nanotubes is proved by a very low filler percolation threshold, comparable with those attainable through much more intensive mixing procedures. The PNCs also exhibit high thermal stability and dynamic mechanical strength at low filler content, which means that the ease of dispersion is achieved preserving the structural integrity of the nanotubes. Our results demonstrate that the synthesis of easily dispersible CNTs represents a viable route for the large-scale production of PNCs of technological interest.

2. Experimental

2.1. Materials

The polymer matrix is atactic polystyrene (PS, Polimeri Europa, Italy) with average molecular weight $M_w = 125$ KDa, polydispersity index $M_w/M_n = 2$, zero-shear rate viscosity $\eta_0 = 1.7 \times 10^3$ Pa s at temperature $T = 200$ °C and glass transition temperature $T_g = 100$ °C. Unfunctionalized MWCNTs are produced by FBCCVD and then purified via a novel three-step process entirely carried out in a single device (details are given in the next section). Commercial grade MWCNTs (Baytubes® C150P, Bayer MaterialScience, Germany), produced by chemical vapor deposition using a metal catalyst, are used as reference material. The main features of the synthesized and commercial nanotubes are summarized in Table 1.

2.2. Synthesis of the nanotubes and preparation of the nanocomposites

Unfunctionalized MWCNTs were synthesized in a large scale (500 g/batch) fluidized bed reactor (diameter 15 cm, height 100 cm) using a γ-alumina substrate impregnated with iron as catalyst [17], ethylene as carbon source, hydrogen and nitrogen as fluidizing agents. The reaction was carried out at $T = 600$ °C and at atmospheric pressure. The reaction was monitored by an on-line gas-chromatograph (Double Channel MicroGC 3000 Agilent) to evaluate in real-time the ethylene conversion and the yield of the reaction; the average duration of the synthesis was about 120 min. Then, the pristine MWCNTs were purified in a three phase slurry bubble vessel through a three-step liquid phase acid treatment: (i) refluxing sulfuric acid solution to dissolve catalyst particles; (ii) water washing to remove the amount of acid; (iii) drying to remove the remaining water. PNCs at different filler content (Φ) were prepared by a two-step melt mixing route. First, a masterbatch at $\Phi \sim 6$ wt.% of MWCNTs was produced using a co-rotating conical twin-screw micro-compounder (Xplore, DSM). The resulting sample was then diluted by melt mixing with neat PS to adjust

Table 1
Main features of the two kinds of MWCNTs.

Property	Synthesized MWCNTs	Commercial MWCNTs
Carbon purity	>99%[a]	⩾95%[b]
Outer mean diameter	~10 nm[c]	~10.5 nm[d]
Mean length	~720 nm[e]	~770 nm[d]
I_D/I_G ratio[f]	1.21 ± 0.15	1.22 ± 0.04
Aggregates average size	103 ± 63 μm[g]	382 ± 122 μm[g]
Bulk density	90–120 Kg m^{-3}[h]	130–150 Kg m^{-3}[b]

[a] From TGA analyses.
[b] Taken from Ref. [15].
[c] From image analysis of TEM micrographs.
[d] Taken from Ref. [2].
[e] From image analysis of TEM micrographs following the same procedure as described in Ref. [16].
[f] Ratio between the intensity of the D (1280–1350 cm^{-1}) and G (1580–1600 cm^{-1}) bands as deduced through Raman spectroscopy.
[g] From particles size analysis.
[h] According to EN ISO 60 norm.

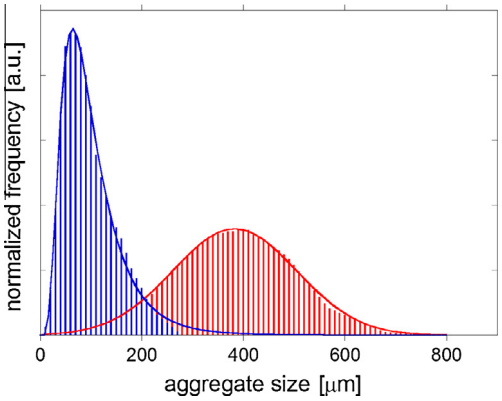

Fig. 1. Normalized size distribution functions of synthesized (blue) and commercial (red) CNT aggregates. Solid lines are Lognormal and Gaussian fittings, respectively. (For interpretation of the references to color in this figure legend, the reader is referred to the web version of this article.)

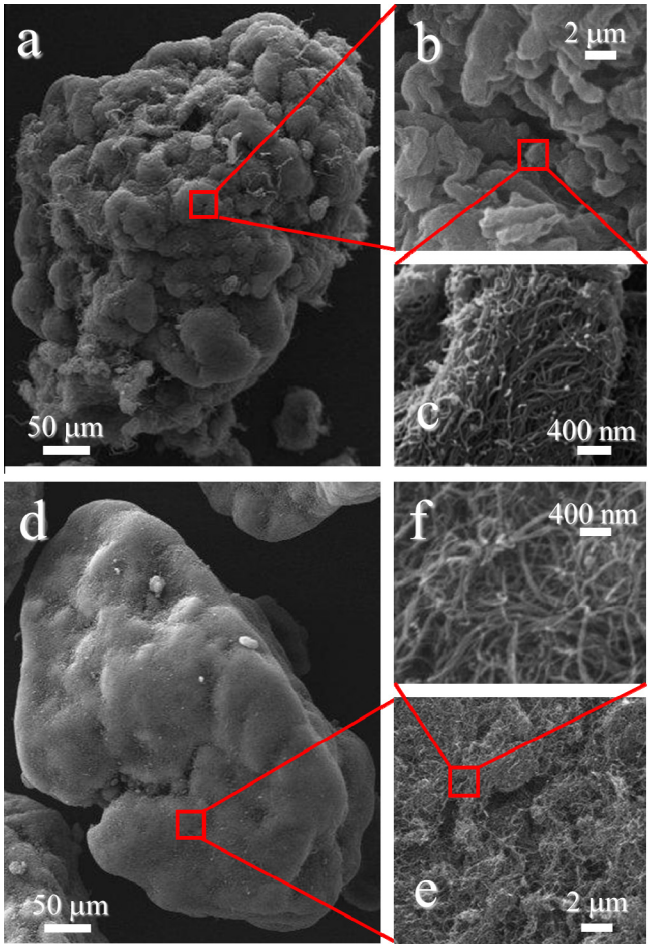

Fig. 2. SEM micrographs of the primary aggregates of the (a–c) synthesized and (d–f) commercial CNTs on different length scales.

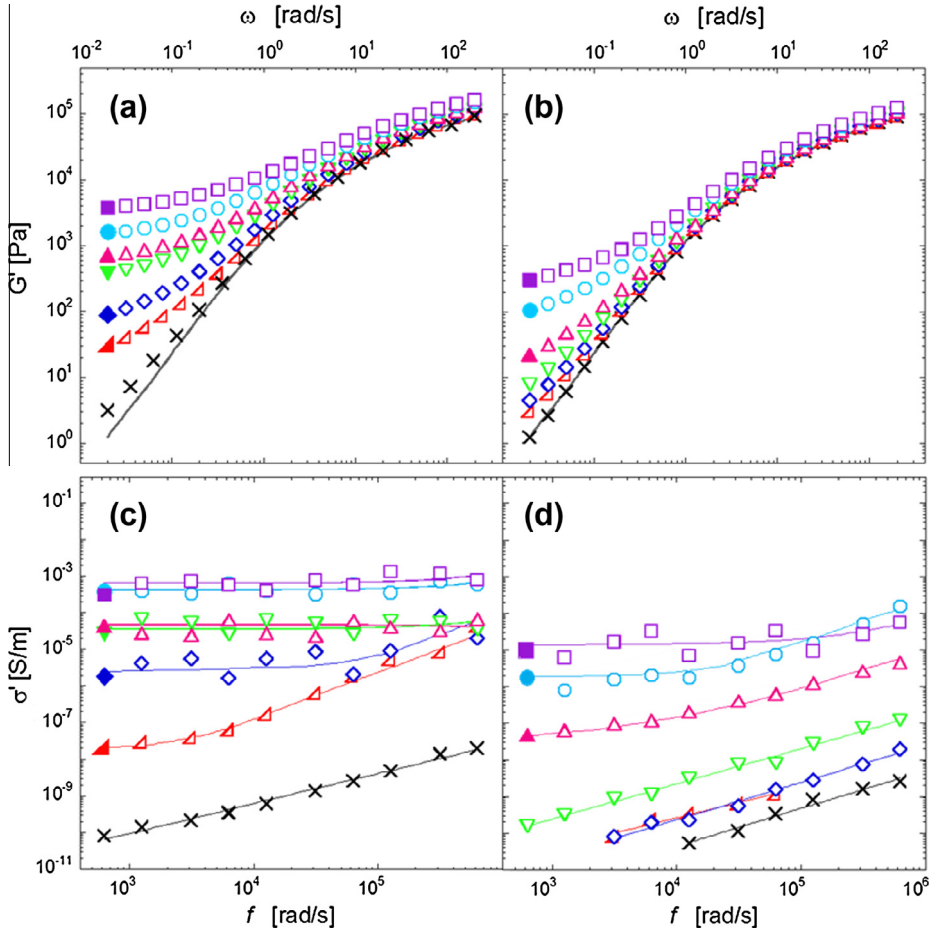

Fig. 3. (a and b) ω-Dependent elastic modulus and (c and d) f-dependent real conductivity of the nanocomposites filled with (a and c) synthesized and (b and d) commercial nanotubes at different compositions. From bottom to top: (a and c) Φ = 0.07, 0.20, 0.42, 0.73, 0.95, 1.36, 1.81 wt.%; (b and d) Φ = 0.11, 0.32, 0.62, 0.80, 1.13, 1.44, 2.07 wt.%. Solid lines in *a* and *b* represent the G' of the neat PS; in *c* and *d* are guides for the eye. Full symbols represent the G'_0 (a and b) and the σ_{DC} (c and d) of the samples above the Φ_c.

the composition. The extrusions were all performed at T = 200 °C in nitrogen atmosphere at a screw speed of 200 rpm, corresponding to average shear rates of ~75 s^{-1}. Finally, the extrudate was compression-molded into disks (diameter 40 mm, thickness ~1.5 mm) for the subsequent analyses.

2.3. Characterization

Transmission electron microscopy (TEM, Tecnai G2 Spirit Twin T-12 by FEI) was carried out on the pristine powders to evaluate the diameter and length of the single CNTs. Scanning electron microscopy (SEM, ZEISS EVO 50 EP apparatus) was performed on the dry CNT powders to investigate the morphology of the primary aggregates. A CILAS 1180 L particle size analyzer was used to assess the dimensions of the primary aggregates. TEM analyses on the PNCs were performed using a Philips EM208 apparatus. The observations were carried out on ~150 nm-thick slices cut at room temperature using a diamond knife. Rheological tests were performed in dry nitrogen atmosphere at T = 180 °C using a stress-controlled rotational rheometer (ARG2, TA Instruments) in parallel-plate geometry (diameter d = 40 mm). First, low-frequency ($\omega = 10^{-1}$ - rad/s) time-sweep experiments were carried out. After the reaching of the steady state, the elastic (G') and viscous (G'') shear moduli were measured as a function of mechanical frequency in the linear regime, which was previously evaluated for each composition through strain amplitude tests. Dielectric spectroscopy was performed at room temperature on the disks recovered at the end of rheological tests. Measurements were carried out using a rotational rheometer (ARES, Rheometrics Scientific) equipped with a dielectric thermal analysis tool, constituted by a couple of stainless steel parallel plates (d = 25 mm) connected with a LCR Meter (E4980A, Agilent). The real (ε') and imaginary (ε'') parts of the complex permittivity were monitored as functions of the frequency of the electrical field, f. The measurements were repeated five times per sample. The real part of the complex conductivity was estimated as $\sigma' = \varepsilon'' \cdot \varepsilon_0 \cdot f$, where $\varepsilon_0 = 8.85 \times 10^{-12}$ F m^{-1} is the permittivity of free space. Thermogravimetric analyses were performed using a Q5000 TGA apparatus (TA Instruments). The samples were heated up to T = 700 °C at 10 °C min^{-1} in nitrogen atmosphere. The onset of thermal degradation, identified as the temperature at which a weight loss of 5 wt.% occurred ($T_{5\%}$), and the temperature of maximum rate of degradation (T_{peak}) were recorded. The actual content of nanotubes in the PNCs was estimated as the residual weight at T = 550 °C. Dynamic mechanical analyses were carried out using a Tritec 2000 DMA apparatus (Triton Technology Ltd., Grantham). The elastic (E') and viscous (E'') flexural moduli were measured as function of temperature in single-cantilever bending mode at a frequency of 1 Hz and with a total displacement of 0.02 mm, which is small enough to be in the linear regime. The sample bars ($10 \times 20 \times 1$ mm^3) were heated at 2 °C min^{-1} from room temperature. Three independent measurements were carried out for each sample.

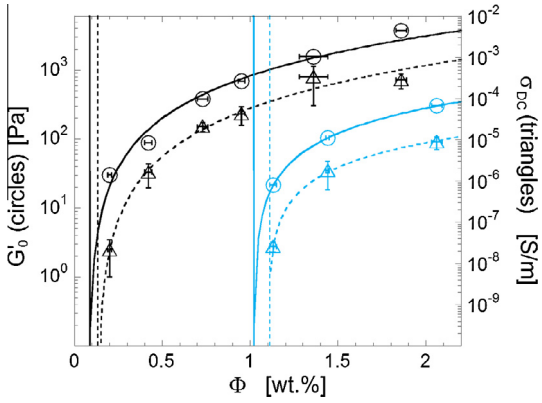

Fig. 4. Φ-Dependence of the network elasticity (circles) and the DC electrical conductivity (triangles) for the nanocomposites filled with synthesized (black) and commercial (blue) nanotubes. Lines are power law fittings. (For interpretation of the references to color in this figure legend, the reader is referred to the web version of this article.)

3. Results and discussion

3.1. Morphology and structure of the primary aggregates

The normalized size distribution functions (SDF) of the dry powders are reported in Fig. 1 for the two kinds of CNTs. The average size of the aggregates is much smaller for the synthesized particles. Such a parameter, however, is not strictly related to the dispersibility of CNTs in polymer matrices [18]. More important, the SDF of the commercial nanotubes results much wider. The small aggregates fill up the space between the big ones, thus affecting the value of bulk density of the powder. The latter is often taken as indicative of the bulk density of the single aggregate, ρ_a, which is known to be a relevant parameter in the dispersion process of CNTs [13]. Actually, ρ_a only partially reflects the actual space arrangement of the single nanotubes inside the aggregates, which ultimately governs the dispersibility. SEM micrographs showing the internal structure of the two kinds of aggregates are reported in Fig. 2. The synthesized CNTs are in the form of loosely packed agglomerates with coarse-grained texture (Fig. 2a), which is likely to facilitate the infiltration of the polymer in the earlier stages of melt mixing. Such an "opened" structure persists also on micro-scale (Fig. 2b), reflecting the presence of interwoven bundles of combed yarns of nanotubes (Fig. 2c). Such an aligned arrangement on nanoscale is expected to favor the pulling out of the nanotubes required for their individualization when melt mixed with polymer matrices. In contrast with the hierarchical structure of the synthesized particles, the aggregates of commercial CNTs appear as fine-textured blocks (Fig. 2d), whose apparent dense structure is the result of a random arrangement of highly entangled, thus difficult to unravel, nanotubes (Fig. 2e and f).

3.2. Estimate of the percolation threshold in the PNCs

The structural and morphological differences between the aggregates of the two kinds of fillers affect the quality of their dispersion within the host polymer. Linear viscoelastic analyses and dielectric spectroscopy are used to assess the percolation thresholds of the two kinds of nanotubes in the PNCs. Before measurements, the samples have been annealed for about 2 h at $T = 220$ °C under gaseous nitrogen. Driven by particle–particle attraction, the re-agglomeration of the filler eventually results in time-independent viscoelastic and dielectric properties [19], which we study as a function of the mechanical and electrical frequency.

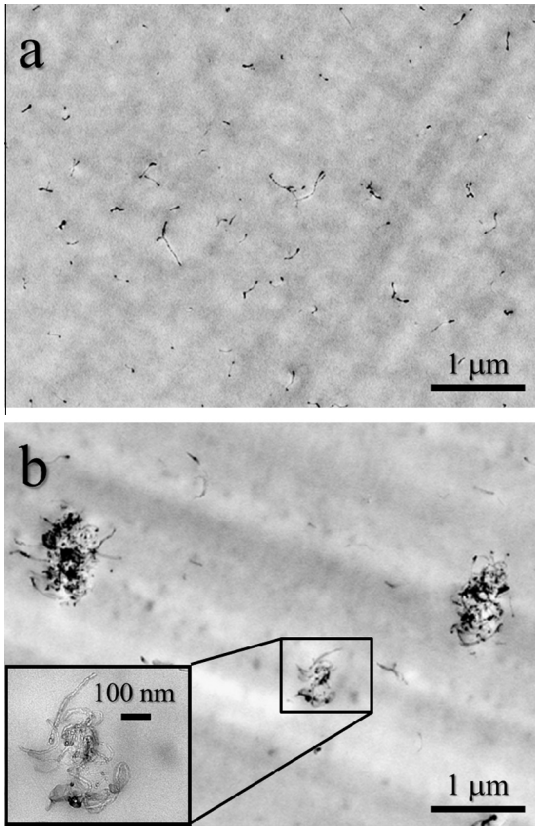

Fig. 5. TEM micrographs of nanocomposites at (a) $\Phi = 0.07$ wt.% of synthesized nanotubes and (b) at $\Phi = 0.32$ wt.% of commercial ones.

The elastic modulus G', more sensitive than G'' to the state of dispersion of the nanotubes, is shown in Fig. 3a and b for PNCs based on synthesized and commercial CNTs, respectively. The two systems share the same qualitative behavior, peculiar of many PNCs. In particular, the flattening of G' at low frequency indicates the occurrence of a liquid- to solid-like rheological transition due to the formation of an elastic network of CNTs [20]. The comparison between the two families of curves reveals that higher contents of worse dispersed commercial CNTs are required to obtain comparable enhancements of G' as those attained in the case of synthesized nanotubes. Similar conclusions can be drawn looking at the real part of the complex conductivity shown in Fig. 3c and d. The appearance of the low-frequency plateau of σ' is indicative of an insulator–conductor transition, which reflects the formation of a percolating network of conductive particles. The system based on the synthesized CNTs experiences such a transition at some Φ in the range 0.07–0.20 wt.%, whereas the critical content of the

Table 2
Rheological and electrical percolation thresholds and corresponding fitting parameters.

	$G'_0 = k(\Phi - \Phi_c^r)^v$			$\sigma_{DC} = \sigma_0(\Phi - \Phi_c^e)^t$		
	Φ_c^r (wt.%)	k (Pa)	v	Φ_c^e (wt.%)	$\sigma_0 \times 10^6$ (S/m)	t
PS/synthesized CNTs	0.08 ± 0.01	969 ± 17	1.8 ± 0.1	0.13 ± 0.05	91.3 ± 34.8	3.1 ± 0.8
PS/commercial CNTs	1.02 ± 0.05	289 ± 16	1.2 ± 0.1	1.10 ± 0.09	10.3 ± 5.1	1.7 ± 0.5

commercial ones falls in the range 0.8–1.13 wt. To estimate more accurately the percolation thresholds, the percolation theory has been exploited. Both the network elasticity, G_0', and DC conductivity, σ_{DC}, are known to grow with Φ as:

$$Y = a(\Phi - \Phi_c)^b \quad (\text{for } \Phi > \Phi_c) \tag{1}$$

where Y represents either G_0' or σ_{DC}, and a and b are parameters related to the mechanisms of stress bearing or electrical transport [21]. Eq. (1) has been fitted to the values of G' and σ' at the lowest investigated frequencies, which we take as representative of the network elasticity and DC conductivity, respectively. Incrementally varying Φ_c in the composition ranges previously identified, the rheological, Φ_c^r, and electrical, Φ_c^e, percolation thresholds are set as the values which return the maximum regression coefficient R^2. The results of the fitting procedure are shown in Fig. 4, and the computed parameters are summarized in Table 2.

Electrical percolation requires direct contact between nanotubes, whereas mechanical interactions among particles may take place via the mediation of shells of confined or adsorbed polymer chains. Consequently, in both systems the value of Φ_c^e results slightly higher than Φ_c^r. In any case, the better dispersibility of the synthesized CNTs clearly emerges from the comparison of the percolation thresholds. Besides being about one order of magnitude lower than that of the commercial nanotubes, the Φ_c of the system based on synthesized particles is among the lowest reported in the literature for polystyrene–CNT nanocomposites, irrespective of the adopted compounding technique [22]. We stress that such a result has been obtained without the optimization of the processing parameters, whose fine tuning is known to be important for enhancing the dispersion of CNTs inside polymer matrices [23]. Finally, the comparison between the values of the critical exponents v and t reported in Table 2 reveals that both the strength and electrical conductivity of the network grow with Φ more rapidly for the synthesized CNTs. This is ascribed to the different structures of the percolating networks, which are based on distinct building blocks. To isolate such basic elements, TEM analyses have been performed on two diluted samples with comparable viscoelastic and dielectric features. Individualized nanotubes and small clusters can be noticed in the case of synthesized particles (Fig. 5a), whereas the presence of bigger entangled hanks characterizes the sample based on commercial nanotubes (Fig. 5b). The former, smaller and better distributed in the space, are expected to be more effective in contributing to the mechanical and electrical properties of the network.

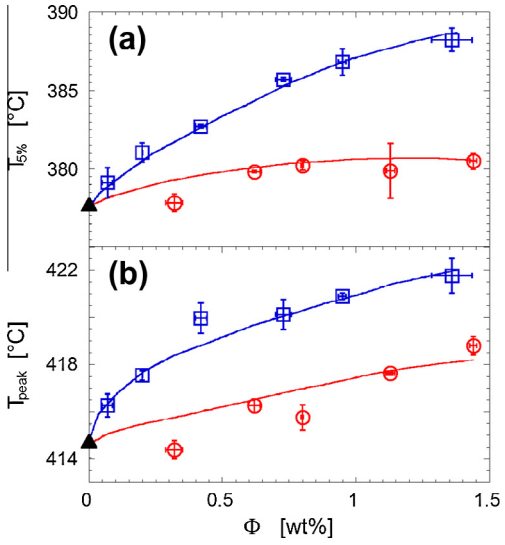

Fig. 6. Φ-Dependence of (a) $T_{5\%}$ and T_{peak} of the nanocomposites filled with synthesized (squares) and commercial (circles) CNTs. The full triangle represent the neat PS and the solid lines are guide for the eye.

3.3. Thermal and dynamic mechanical analyses

The very low percolation threshold detected for the PNCs based on synthesized particles reveals that the nanotubes are well dispersed inside the host polymer matrix. To demonstrate that such a result has not been obtained to the detriment of the integrity of the CNTs, the thermal stability and dynamic mechanical response have been investigated. Nanotube breakage, in fact, would negatively reflect on the macroscopic properties of the PNCs [11]. The results of TGA are summarized in Fig. 6 in terms of onset of thermal degradation (Fig. 6a) and temperature of maximum rate of degradation (Fig. 6b) for the two families of PNCs. Besides being systematically higher, both $T_{5\%}$ and T_{peak} grow with Φ more rapidly for the nanocomposites based on the synthesized nanotubes. Again, such a higher sensitivity to filler content reflects a finer and more homogeneous dispersion of the particles. Similar conclu-

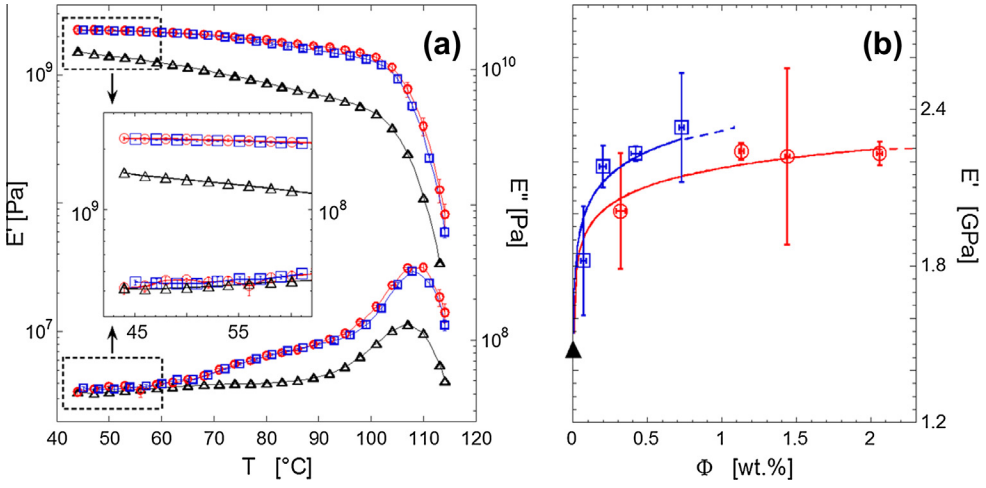

Fig. 7. (a) T-dependence of E' and E'' for the neat PS (triangles) and for nanocomposite at $\Phi \sim 0.4$ wt.% of synthesized CNTs (squares) and at $\Phi \sim 2.0$ wt.% of commercial ones (circles). (b) Φ-Dependence of E_g' for the nanocomposites filled with synthesized (squares) and commercial (circles) CNTs. The full triangle represent the neat PS and the solid lines are guide for the eye.

sions can be drawn for the dynamic-mechanical properties. The viscoelastic moduli are shown in Fig. 7a as a function of temperature for the neat PS and two representative PNCs above their percolation thresholds. The overall effect of the two kinds of filler is similar, the moduli of the PNCs being higher than those of the neat polymer except for E'' at low temperature. The high dispersibility of the synthesized particles ensures the same enhancements at much lower CNT loadings. We observe that dealing with small amounts of particles is also desirable because too large amounts of filler can deteriorate the ultimate mechanical properties of the nanocomposite [24]. Focusing on the glassy modulus, E'_g, which is reported in Fig. 7b as a function of filler content, we still notice a faster growth with Φ for the samples based on the synthesized CNTs. Negligible enhancements of the mechanical properties are usually observed for melt processed MWCNT-filled composites, especially for brittle matrices such as polystyrene [25]. Nonetheless, an increase of about 50% is obtained upon addition of only ~0.4 wt.% of synthesized CNTs. It is important to stress that such a result is exclusively due to the reinforcing action of the CNTs. The amorphous nature of our matrix, in fact, excludes possible contributions of a crystalline phase which may enucleate in the proximity of the CNT walls [26].

4. Conclusions

The dispersibility of MWCNTs synthesized by fluidized bed catalytic chemical vapor deposition and purified through a scalable one-pot route has been investigated focusing on the role of the morphology and structure of the primary CNT aggregates. Commercially available nanotubes with the same features but differently arranged in the aggregates have been used as reference. Specifically, the synthesized particles are in the form of small and loosely packed clusters made by interwoven bundles of combed yarns of nanotubes. Differently, the aggregates of the commercial particles appear as bigger blocks, whose fine-textured surface is the result of a random arrangement of highly entangled nanotubes. Polystyrene-based nanocomposites at different particle loading were prepared through a mild masterbatch melt mixing route. The peculiar hierarchical structure of the synthesized particles results in a superior dispersibility in the host polymer matrix, as confirmed by both rheological measurements and dielectric spectroscopy. In particular, the CNT percolation threshold in the nanocomposites filled with the synthesized particles is resulted one order of magnitude lower than that attained with the commercial ones, and is among the lowest reported in the literature for PS–CNT nanocomposites. Such a result is not achieved to the detriment of the nanotube integrity, and the nanocomposites exhibit enhanced thermal stability and dynamic mechanical properties. In particular, a noticeable enhancement the glassy modulus has been achieved at low amounts of CNTs (~0.4 wt.%) despite the brittle and amorphous nature of the polymer matrix.

Acknowledgments

The authors thank Dr. G. Gentile for TEM observations and Drs. Pellegrino Musto and Pietro La Manna for Raman spectroscopy analyses carried out at the laboratories of the Italian National Research Council. This work has been supported by the Italian Ministry of University and Research (MIUR) through the PRIN 2009 prot. 2009WXXLY2_002.

References

[1] Lin B, Sundararaj U, Pötschke P. Melt mixing of polycarbonate with multi-walled carbon nanotubes in miniature mixers. Macromol Mater Eng 2006;291:227–38.
[2] Castillo FY, Socher R, Krause B, Headrick R, Grady BP, Prada-Silvy R, et al. Electrical, mechanical, and glass transition behavior of polycarbonate-based nanocomposites with different multi-walled carbon nanotubes. Polymer 2011;52(17):3835–45.
[3] Alig I, Pötschke P, Lellinger D, Skipa T, Pegel S, Kasaliwal GR, et al. Establishment, morphology and properties of carbon nanotube networks in polymer melts. Polymer 2012;53:4–28.
[4] Sahoo NG, Rana S, Cho JW, Li L, Chan SH. Polymer nanocomposites based on functionalized carbon nanotubes. Prog Polym Sci 2010;35(7):837–67.
[5] Grady BP. Recent developments concerning the dispersion of carbon nanotubes in polymers. Macromol Rapid Commun 2010;31:247–57.
[6] Krause B, Ritschel M, Täschner C, Oswald S, Gruner W, Leonhardt A, et al. Comparison of nanotubes produced by fixed bed and aerosol-CVD methods and their electrical percolation behaviour in melt mixed polyamide 6.6 composites. Compos Sci Tech 2010;70:151–60.
[7] Krause B, Villmow T, Boldt R, Mende M, Petzold G, Pötschke P. Influence of dry grinding in a ball mill on the length of multiwalled carbon nanotubes and their dispersion and percolation behaviour in melt mixed polycarbonate composites. Compos Sci Technol 2011;71:1145–53.
[8] Shokrieh MM, Rafiee R. Investigation of nanotube length effect on the reinforcement efficiency in carbon nanotube based composites. Compos Struct 2010;92(10):2415–20.
[9] Morcom M, Atkinson K, Simon GP. The effect of carbon nanotube properties on the degree of dispersion and reinforcement of high density polyethylene. Polymer 2010;51(15):3540–50.
[10] Socher R, Krause B, Boldt R, Hermasch S, Wursche R, Pötschke P. Melt mixed nanocomposites of PA12 with MWNTs: influence of MWNT and matrix properties on macrodispersion and electrical properties. Compos Sci Technol 2011;71(3):306–14.
[11] Pegel S, Pötschke P, Petzold G, Alig I, Dudkin SM, Lellinger D. Dispersion, agglomeration, and network formation of multiwalled carbon nanotubes in polycarbonate melts. Polymer 2008;49(4):974–84.
[12] Krause B, Petzold G, Pegel S, Pötschke P. Correlation of carbon nanotube dispersability in aqueous surfactant solutions and polymers. Carbon 2009;47(3):602–12.
[13] Krause B, Mende M, Pötschke P, Petzold G. Dispersability and particle size distribution of CNTs in an aqueous surfactant dispersion as a function of ultrasonic treatment time. Carbon 2010;48(10):2746–54.
[14] Verge P, Benali S, Bonnaud L, Minoia A, Mainil M, Lazzaroni R, et al. Unpredictable dispersion states of MWNTs in HDPE: a comparative and comprehensive study. Eur Polym J 2012;48(4):677–83.
[15] Bayer MaterialScience AG. Product Information Baytubes® C150P. Edition 2008-03-10.
[16] Krause B, Boldt R, Pötschke P. A method for determination of length distributions of multiwalled carbon nanotubes before and after melt processing. Carbon 2011;49(4):1243–7.
[17] Mazzocchia CV, Bestetti M, Acierno D, Tito AC. European patent 2010; 2213369.
[18] Bai JB, Allaoui A. Effect of the length and the aggregate size of MWNTs on the improvement efficiency of the mechanical and electrical properties of nanocomposites – experimental investigation. Compos Part A 2003;34:689–94.
[19] Alig I, Skipa T, Lellinger D, Pötschke P. Destruction and formation of a carbon nanotube network in polymer melts: rheology and conductivity spectroscopy. Polymer 2008;49(16):3524–32.
[20] Filippone G, Salzano de Luna M. A unifying approach for the linear viscoelasticity of polymer nanocomposites. Macromolecules 2012;45(21):8853–60.
[21] Stauffer D, Aharony A. Introduction to percolation theory. 2nd ed. London: Taylor & Francis; 1992.
[22] Bauhofer W, Kovacs JZ. A review and analysis of electrical percolation in carbon nanotube polymer composites. Compos Sci Technol 2009;69:1486–98.
[23] Villmow T, Kretzschmar B, Pötschke P. Influence of screw configuration, residence time, and specific mechanical energy in twin-screw extrusion of polycaprolactone/multi-walled carbon nanotube composites. Compos Sci Technol 2010;70:2045–55.
[24] Zhou K, Gu S-Y, Zhang Y-H, Ren J. Effect of dispersion on rheological and mechanical properties of polypropylene/carbon nanotubes nanocomposites. Polym Eng Sci 2012;52(7):1485–94.
[25] Spitalsky Z, Tasis D, Papagelis K, Galiotis C. Carbon nanotube–polymer composites: chemistry, processing, mechanical and electrical properties. Prog Polym Sci 2010;35(3):357–401.
[26] Logakis E, Pandis C, Pissis P, Pionteck J, Pötschke P. Highly conducting poly(methyl methacrylate)/carbon nanotubes composites: investigation on their thermal, dynamic-mechanical, electrical and dielectric properties. Compos Sci Tech 2011;71(6):854–62.